LATH STRUCTURED MONAZITE FROM HAUHGTON DOME, CANADA REVEALS SHOCK-INDUCED TETRAGONAL HIGH PRESSURE POLYMORPH OF $REEPO_4$. T. M. Erickson[1†,2] N. E. Timms[2], M. Pearce[3], C. Cayron[4], L. P. Keller[1] and A. Deutsch[6] [1]Astromaterials Research and Exploration Science division, NASA Johnson Space Center, 2101 NASA Parkway, Houston, TX, 77058, USA [†]Jacobs – JETS (Timmons.m.erickson@nsaa.gov), [2] Curtin University, GPO Box 1984, Perth, WA, 6845, Australia, [3]CSIRO Mineral Resources, 26 Dick Perry Avenue, Kensington, WA, 6151, Australia, [4]École Polytechnique Fédérale de Lausanne (EPFL), Rue de la Maladière 71b, 2000 Neuchâtel, Switzerland, [5]Westfälische Wilhelms-Universität Münster, Wilhelm-Klemm-Straße 10, D-48149 Münster, Germany

Introduction: Shock deformed monazite, monoclinic rare earth element (REE) phosphate, from the Haughton Dome impact structure, Nunavut, Canada, contain lath-structured lamellae. Microstructural phase heritage indicate the former presence of a previously unreported, shock-produced, tetragonal-structured, high pressure polymorph of $REEPO_4$.

This study presents an electron backscatter diffraction (EBSD) and transmission electron microscopy (TEM) study of shock deformed monazite from the historic sample DIG-9, a shock stage III, biotite sillimanite gneiss sample from near the central uplift of the Haughton Dome (75°22'20"N, 89°40'50"W), in which shock features in monazite were first described [1].

Analytical methods: After crushing, milling, magnetic and density separation monazite grains were mounted in 25.5 mm epoxy rounds and given a 50 nm final chemical-mechanical polish using a colloidal silica dispersion. Individual grains were imaged with a JEOL 7600F field emission gun (FEG) scanning electron microscope (SEM)and then mapped using 200- and50-nm step sizes with an Oxford Instruments Symmetry™ EBSD system attached to the 7600 FEG SEM. Focused ion beam foils were then prepared from regions of interest and analyzed with a JEOL 2500SE TEM and by transmission Kikuchi diffraction (TKD) using the Symmetry system.

Results: Microstructural EBSD analyses of the shocked monazite grains reveal a variety textures including low-angle grain boundaries, cumulative plastic strain, deformation twins in (001), (100) and (101), and complex lamellae containing differently-oriented interlocking laths of monazite (Fig. 1). Each complex lamella is made up of interlocking monazite laths with up to four crystallographic orientations that are systematically disoriented from the host monazite grain described by 18° <001>, 180° <301>, and two conjugate sets about 90° <301>. Each of the four laths also share the pole to (100) with each other and are disoriented from one another by either 180°<100> or 90°<401>. All orientation relationships except 180°<100> are inconsistent with disorientation relationships of known deformation twin modes in monazite [2]. Furthermore, the complexity of this type of microstructure cannot be explained simply by deformation twinning.

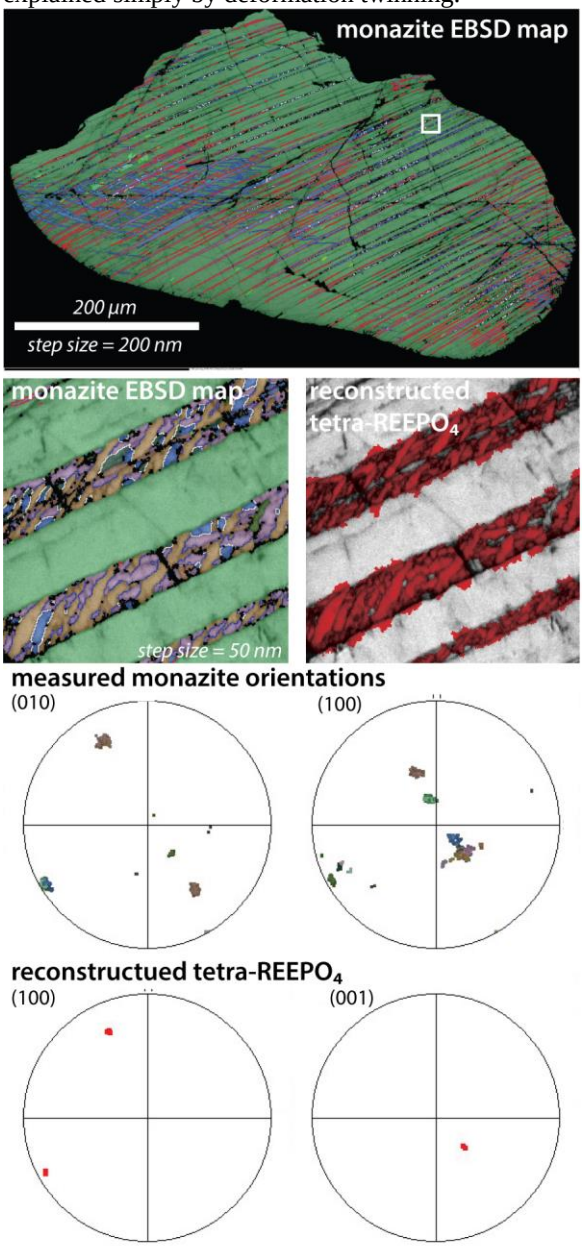

Figure 1. EBSD maps and pole figures of lath structured monazite and reconstructed tetragonal $REEPO_4$.

Transmission electron microscopy analyses reveal alternating domains of the host monazite with lath-structured lamellae, between which, [121] of the host is coincident with the [001] of the lath-structured domains. The host monazite contains numerous dislocations, low angle grain boundaries, and deformation twins. The interface between the lath-structured material and the host domains consists of complex subgrains, voids, and pockets of impact-melt (Fig. 2a). Grain boundaries between the lath-structured monazite lamellae are bounded by (100) stacking faults (Fig. 2b).

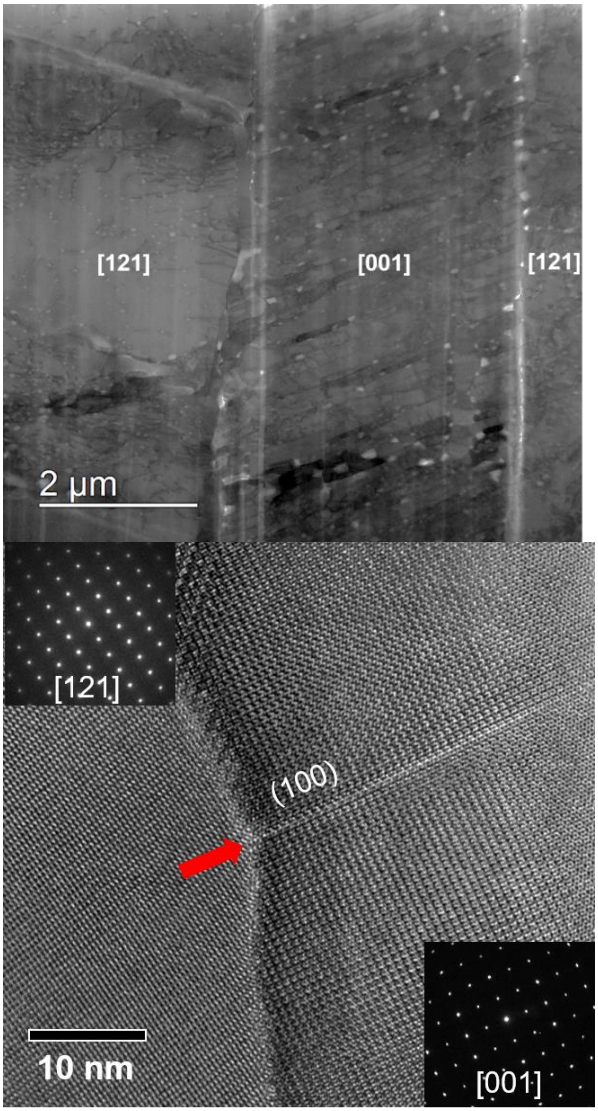

Figure 2. A. Bright field TEM images of host and lath-structured lamellae of monazite. B. High-resolution TEM image of the interface between the [121] host monazite (left) and the [001] lath-structured monazite (right). The red arrow indicates a (100) stacking fault separating two laths.

Phase reconstruction: The lath-structured monazite lamellae resemble microstructures in martensitic steel [e.g. 3] and therefore we investigated a possible phase transformation mechanism for their production. By considering the common directions and planes shared between the laths we inferred that the data reveal a tetragonal parent phase that produces an interphase misorientation relationship whereby $[010]_{monoclinc}$ // $[100]_{tetragonal}$ and $(100)_{monoclinic}$ // $(001)_{tetragonal}$. The orientations of the four monoclinic variants inherited from the tetragonal parent phase were then simulated using the GenOVa program [4], and the theoretical tetragonal-monoclinic phase transformations was processed with the ARPGE program [5] to reconstruct the preexisting parent tetragonal grains (e.g. Fig. 1). Close agreement between the experimental and theoretical phase reconstruction support the interpretation that the interlocking lath microstructure are indeed a reversion product from single-orientation lamellae of a previously undescribed tetragonal (La, Ce, Th)PO_4 polymorph.

Conclusions: These results unequivocally show that the shocked monazite underwent a transformation to a tetragonal-structured phase. As this microstructure has never been observed in endogenically-deformed monazite grains yet is reported here in shock stage III crystalline target rocks, we propose this is a newly discovered shock-pressure-induced transformation of monazite to a previously undescribed phase. The lamellar microstructure formed by phase transformation to tetragonal (La, Ce, Th)PO_4 is consistent with a deviatoric (or shear-type) transformation, such as has been described for the zircon to reidite transformation in the $ZrSiO_4$ system [5]. However, our observations suggest that the energetics of the transformation to a tetragonal polymorph indicate that this phase will inevitably be reverted back to monazite upon decompression. Because the solid-state reversion to monoclinic monazite is crystallographically-controlled the previous existence of this phase can be revealed by quantitative misorientation analysis.

References: [1] Schärer, U. and Deutsch, A. (1990) *GCA, 54*, 3435–3447. [2] Erickson T. M. et al. (2016) *Geology, 44*, 635–638. [3] Cayron C. et al. (2006) *Materials Characterization, 57*, 386–401. [4] Cayron (2007) *J. Applied Crystallography, 40*, 1179–1182. [4] Cayron (2007) *J. Applied Crystallography, 40*, 1183–1188. [5] Erickson et al. (2017) *CMP, 172*.